INTERFACE SCIENCE 12, 19–27, 2004

Geometric and Crystallographic Characterization of WC Surfaces and Grain Boundaries in WC-Co Composites

CHANG-SOO KIM AND GREGORY S. ROHRER*
Department of Materials Science and Engineering, Carnegie Mellon University, Pittsburgh, PA 15213, USA
gr20+@andrew.cmu.edu

Abstract. Electron backscattered diffraction has been used to determine the orientation of WC crystals in a WC-Co composite and atomic force microscopy has been used to measure the shapes of planar sections of the same crystals. A stereological analysis has been used to determine that $\{10\bar{1}0\}$ prism facets and the $\{0001\}$ basal planes are the WC surfaces that are most frequently in contact with Co. Further, the WC habit is an approximately equiaxed trigonal prism bound by three prism facets and two basal facets. An analysis of ∼15,600 grain boundaries shows that certain interfaces occur with a frequency that is much higher than would be expected in a random distribution and that the grain boundary habit planes also have $\{10\bar{1}0\}$ and $\{0001\}$ orientations. Eleven percent of all the observed WC-WC interfaces are 90° twist boundaries about $[10\bar{1}0]$. Two types of boundaries with a 30° rotation about [0001], a twist and an asymmetric tilt, comprise 3% of the population.

Keywords: Tungsten carbide, crystal shape, grain boundaries, composite, stereology

Introduction

WC-Co composites have a combination of hardness and toughness that make them useful for machining, mining, construction, and other applications where it is necessary to shape, cut, or crush hard materials [1, 2]. A typical WC-Co composite will contain 70 to 90 volume percent (v/o) of WC crystals in Co matrix. In these composites, there are Co-Co boundaries, WC-WC boundaries, and WC-Co boundaries. The focus of this paper is on the crystallographic distribution of WC-Co and WC-WC boundaries. Here, we employ a recently proposed stereological technique that combines orientation data, measured by electron back scattered diffraction, and geometric data measured by atomic force microscopy (AFM), to determine the habit planes of surfaces and grain boundaries in WC-Co composites [3].

Based on the observation of deeply etched samples, the WC habit has been identified both as a trigonal prism, with three prismatic and two basal facets, or a truncated trigonal prism, where some of the corners or edges of the trigonal prism are replaced by new facets [2, 4, 5]. Therefore, this composite system is a good practical test for the new stereology [3]. To what is already known about the WC habit, the current analysis adds quantitative measurements of the relative surface areas of the WC-Co habit planes. Much less is known about the habit planes of WC-WC grain boundaries [6–8]. Based on the inhomogeneous distribution of observed dihedral angles between contiguous WC grains, it has been proposed that certain grain boundaries are not penetrated by Co and, therefore, occur with a higher frequency [2]. By the measurement of grain boundary misorientations, and the stereological analysis of the grain boundary traces on the plane of observation, we demonstrate that there are preferred misorientations and habit planes. Since these boundaries correspond to special geometric arrangements, we surmise that they are also low energy configurations not spontaneously wet by Co and this explains their high frequency of occurrence in the composite structures.

*To whom all correspondence should be addressed.

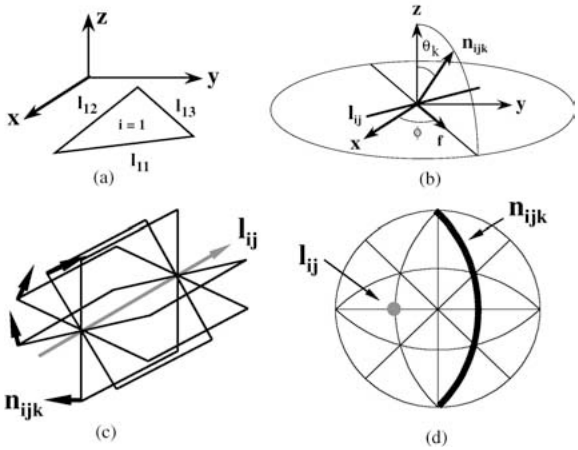

Figure 1. Schematic illustration of the stereological analysis.

Method

Overview

The stereological methods used here have been described in detail in a pervious paper [3]. Here, only a summary of the procedure is presented. In two-dimensional micrographs, sections of faceted crystals appear as polygons, where each line segment, $\mathbf{l_{ij}}$, comes from a different bounding plane (see Fig. 1(a)). While the actual plane that created the observed line segment is unknown, it is certain to belong to the set of planes ($\mathbf{n_{ijk}}$) whose normals are perpendicular to the segment (see Fig. 1(c)). If the crystal orientation (g) is known, then the possible habit planes can be transformed to the crystal reference frame, $\mathbf{n'_{ijk}} = g\mathbf{n_{ijk}}$. On a stereographic projections, the planes $\mathbf{n'_{ijk}}$ lie on a great circle perpendicular to the line segment (see Fig. 1(d)). By observing many segments from different crystals, a corresponding number of sets of possible planes (each on a different great circle) that might be responsible for the observations are also identified. These observations are used to calculate the probability, $p(\mathbf{n'})$, that a given length of line on the perimeter of a random section plane falls on a plane with the orientation $\mathbf{n'}$ according to the following equation:

$$p(\mathbf{n'}) = \frac{\sum_{i,j,k} g_i \mathbf{n_{ijk}} |\mathbf{l_{ij}}| \sin\theta_k}{\sum_{i,j,k} |\mathbf{l_{ij}}| \sin\theta_k}, \qquad (1)$$

where θ_k is defined in Fig. 1(b). The key to this analysis is that correct habit planes are sampled with a high probability; there is at least one habit plane in each set of possible planes, $\mathbf{n_{ijk}}$. Therefore, the great circles arising from each observed line segment must intersect at the positions of habit planes and $p(\mathbf{n'})$ will exhibit local maxima at these positions. Because non-habit planes are far more numerous, any specific non-habit plane is observed much less frequently than a true habit plane.

To determine the crystal shape, it is necessary to know the relative area of each habit plane. Since it is known that the total length of a set of randomly distributed lines intersecting an area is proportional to that area, the ratios of the line lengths associated with each habit plane provides an estimate of the relative surface area [9]. To determine which line segments are associated with each habit plane, we compute the angle (α) between each line segment, $\mathbf{l'_{ij}}$, and each previously identified habit plane, $\mathbf{n'_{hkl}}$, and in the crystal reference frame:

$$\alpha = \cos^{-1}[\mathbf{l'_{ij}} \cdot \mathbf{n'_{hkl}} / (|\mathbf{l'_{ij}}||\mathbf{n'_{ijk}}|)] \qquad (2)$$

For the habit plane of origin, $|\alpha\text{-}90^\circ|$ is ideally 0. In practice, discretization and experimental errors lead to finite values of $|\alpha\text{-}90^\circ|$. Therefore, we assign a line segment to a habit plane whenever $|\alpha\text{-}90^\circ|$ is less than some predetermined tolerance angle, between 3 and 10°. This condition allows us to assign each line length to one of the particular habit planes. After all of the data have been classified in this way, we have the total length of line per habit plane and ratios of these quantities yield the surface area ratio. Here, we apply this method to both WC-Co interfaces and to WC-WC grain boundaries. For the case of WC-WC grain boundaries, the planes in the zone of the boundary trace, $\mathbf{n_{ijk}}$, are transformed to the crystal reference frame once with each of the orientations of the two adjoining crystals.

Experimental

The specimens analyzed here were conventional WC-Co composites with no intentional alloying additions. The sample used for the analysis of WC-Co interfaces contained 20 w/o Co (30.5 v/o) while the sample used for the analysis of WC-WC boundaries contained 6 w/o Co (10 v/o). They were consolidated via liquid phase sintering at approximately 1400°C (20 w/o Co) and 1600°C (6 w/o Co) for 45 min. After polishing, the samples are etched in Murakami's reagent (10 g potassium ferricyanide + 10 g sodium hydroxide in 100 ml distilled water) for 1 min. The reagent preferentially

attacks the WC phase and produces topographic differences at the phase boundaries that lead to sharp contrast in AFM images. In our experience, the vertical sensitivity of the AFM allows the phase boundaries in WC/Co composites to be resolved more clearly than by optical or scanning electron microscopy. This is particularly important for measuring the shapes of the sub-micron crystals that are found in these materials.

A Park Scientific Instruments Cp or a Thermomicroscopes M5 were used for all AFM imaging. Gold-coated, sharpened pyramidal Si_3N_4 probes (Thermomicroscopes ML06A-F) were used to obtain images in contact mode. The crystallographic orientations were determined from orientation imaging microscopy (OIM) images. The OIM system (TexSEM Laboratories, Inc.) is used with a Phillips XL40 FEG scanning electron microscope (SEM). OIM images were obtained at a specimen tilt of 70°, an accelerating voltage of 20 kV and a spot size of 5. Orientations were measured at intervals of 0.2 μm in the 20 w/o Co grade (average grain size of $\sim$1.5 μm), and 1.0 μm in the 6 w/o Co grade (average grain size of $\sim$6 μm). It is important that the AFM images and OIM images are recorded in the same reference frame. This was accomplished by making an intentional scratch on the surface of the specimen. The rotational angle difference of the specimen in the AFM and OIM reference frames is less than 2°.

Analysis

All line segments for the habit plane analysis were obtained by hand tracing the boundary positions in AFM images using a computer mouse; a program automatically records the vector components of each line segment. Each segment is then associated with a set of Euler angles obtained from the OIM image. In both the laboratory and crystal reference frames, the spherical domain of planes was partitioned into equal area cells with the out-of-plane parameter, $\cos\theta$, in the range of -1 to 1 and the in-plane angle, ϕ, in the range between 0 and π. For the analysis of WC-Co interfaces, there were 60 discrete values for each parameter, leading to 3600 equal area cells with an approximate resolution of 3°. The analysis of the WC-WC boundaries was conducted using 36 discrete values for each parameter, leading to 1296 equal area cells with an approximate resolution of 5°. The symmetry operators for the hexagonal system were applied to all of the observed line segments in the crystal reference frame.

The distribution of grain boundary misorientations was determined from OIM images. The orientation data were processed to remove spurious observations using a level five "clean-up" in the OIM software (TexSEM Laboratories, Inc. version 3.03). By averaging all of the orientations within a single grain that were measured with a confidence index (CI) greater than 0.2, a single orientation was assigned to each grain. The orientations of individual adjoining grains (g_a and g_b) were then used to calculate the misorientation ($\Delta g_{ab} = g_a g_b^T$) across each boundary. From the misorientation, the rotation angle ($\omega = \cos^{-1}[(\Delta g_{ii}\text{-}1)/2]$) and components of rotation axis ($\mathbf{R}_i = -\varepsilon_{ijk}\Delta g_{jk}/(2\sin\omega)$) were calculated. In the distributions presented here, the relative population of boundary types is weighted by boundary length.

Results

The microstructures of the two samples are illustrated in Fig. 2. AFM images of the 6 and 20 w/o Co samples are shown beside corresponding OIM inverse pole figures (IPF) maps of the same regions. In the AFM image, the white contrast corresponds to Co, which is topographically higher than the WC after the etch. The Individual WC grains are dissolved at different rates by the etching solution and, therefore, have various shades of darker contrast. The differential etching allows both WC-Co and WC-WC boundaries to be easily identified. In the IPF maps, the Co phase (not indexed in the OIM scans) is indicated as black. Based on an examination of (0001) pole figures, we conclude that the WC crystals exhibit no orientation texture.

There is, however, a strong misorientation texture. The OIM image in Fig. 2(d) shows a portion of a larger data set that defines the orientations of $\sim$8400 WC grains. The misorientation across all of observed WC-WC boundaries ($\sim$15,600) has been determined and Fig. 3 illustrates the relative frequency of occurrence of boundaries with different misorientation angles. For comparison, the distribution expected for randomly misoriented hexagonal crystals is also shown [10]. Note that the experimental distribution shows two peaks, at $\sim$30° and 90°, that are not consistent with the random distribution. To examine the distribution of misorientation axes, the data are plotted in axis-angle space, as illustrated in Fig. 4. Note that at 30°, there is a peak at the position of the [0001] rotation axis and at 90°, there is another peak at the position of the $[10\bar{1}0]$ axis, indicating that boundaries with these two

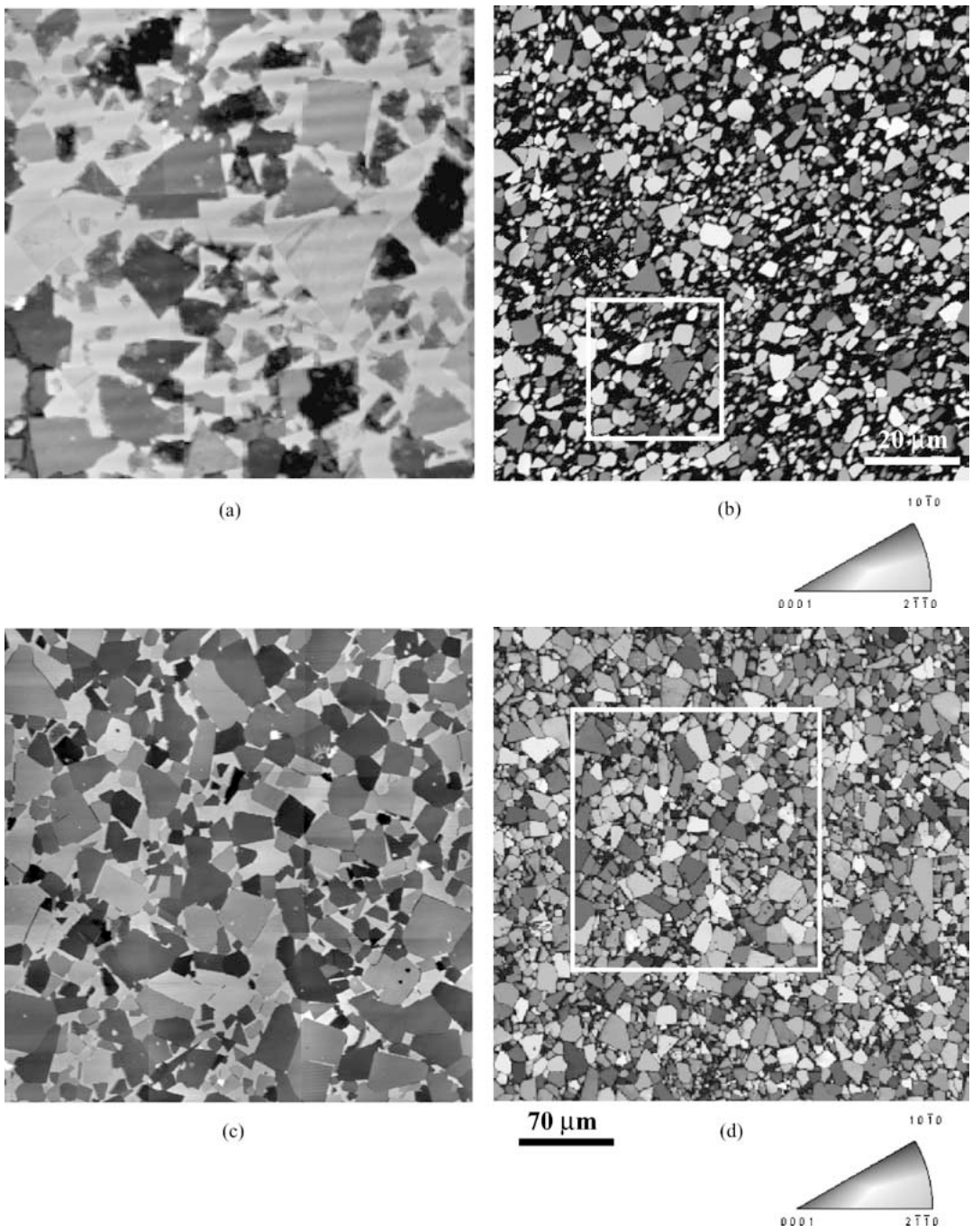

Figure 2. AFM topographic images and OIM inverse pole figure (IPF) maps. (a) AFM image of 20 w/o Co sample ($28 \times 30\ \mu m^2$), (b) OIM IPF map of 20 w/o Co sample ($100 \times 100\ \mu m^2$), (c) AFM image of 6 w/o Co sample ($170 \times 180\ \mu m^2$), and (d) OIM IPF map of 6 w/o Co sample ($350 \times 350\ \mu m^2$).

misorientations occur with a much higher than random frequency.

The habit planes of the WC-Co interfaces and the WC-WC grain boundaries are considered separately. The stereographic projections in Fig. 5 show plots of $p(\mathbf{n}')$ determined from (a) 50 observed crystals and (b) 150 observed crystals. As mentioned earlier, this is the probability that a length of line on the perimeter of an

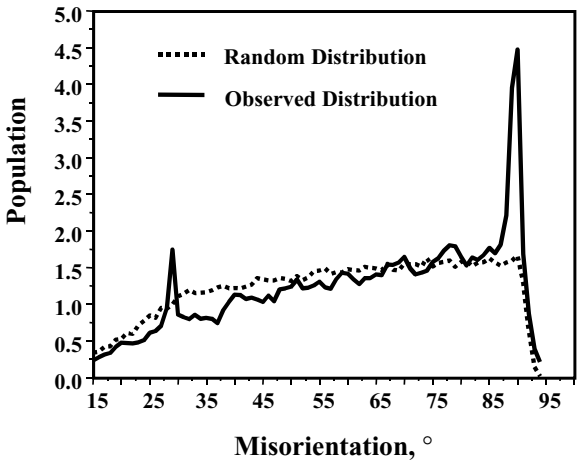

Figure 3. Grain boundary population of WC crystals and random objects as a function of misorientation angle.

observed section of a WC crystal plane was created by a plane with a specific orientation; the results are presented in multiples of a random distribution (MRD). In both cases, the peaks at the {0001} and $\{10\bar{1}0\}$ positions demonstrate that the basal and prism planes dominate the WC crystal habit. To determine what fraction of the observations belong to each habit plane, we computed the angle (α) between each line segment (in the crystal reference frame) and the normals to {0001} and $\{10\bar{1}0\}$. For $|\alpha\text{-}90^\circ| \leq 5^\circ$, 80% of all the observed line segments belong to one of the two habit planes. If the tolerance angle is increased to 10°, then the fraction of observations that can be assigned to either the {0001} and $\{10\bar{1}0\}$ planes increases to 92%. When the 5° tolerance angle is used, which is comparable to the anticipated experimental errors, the basal-to-prism facet area ratio is 0.33. This ratio is not strongly sensitive to α; it varies from 0.31 to 0.34 as the tolerance angle is varied from 3° to 10°.

The results suggest that the average three-dimensional shape of the WC crystal in Co is a hexagonal prism with six indistinguishable $\{10\bar{1}0\}$ prism facets and two {0001} basal facets. To test this assignment, we can inspect the shape of the sections that happen to be oriented parallel or perpendicular to the basal plane. Sections perpendicular to the basal plane should be rectangular and those sections parallel the basal plane should be hexagonal. As illustrated in Fig. 6, those sections perpendicular to {0001} are rectangular, as expected. However, those parallel to the {0001} plane are invariably triangular; hexagonal sections of WC crystals parallel to {0001} are not observed. This indicates that the shape is a trigonal prism bound by only three of the six indistinguishable $\{10\bar{1}0\}$ planes. Considering this shape and the area ratio cited above, the trigonal prism is roughly equiaxed, with an edge length that is 1.14 times the height, as illustrated in Fig. 7. This shape is consistent with earlier observations reported for similar alloys [2, 4, 5].

We can also analyze the habit planes of the boundaries that have a 30° rotation around the [0001] axis and those that have a 90° rotation about the $[10\bar{1}0]$ axis. Here, we consider the bounding plane of each crystal independently. In other words, in the analysis of the line segments, we are applying the complete hexagonal

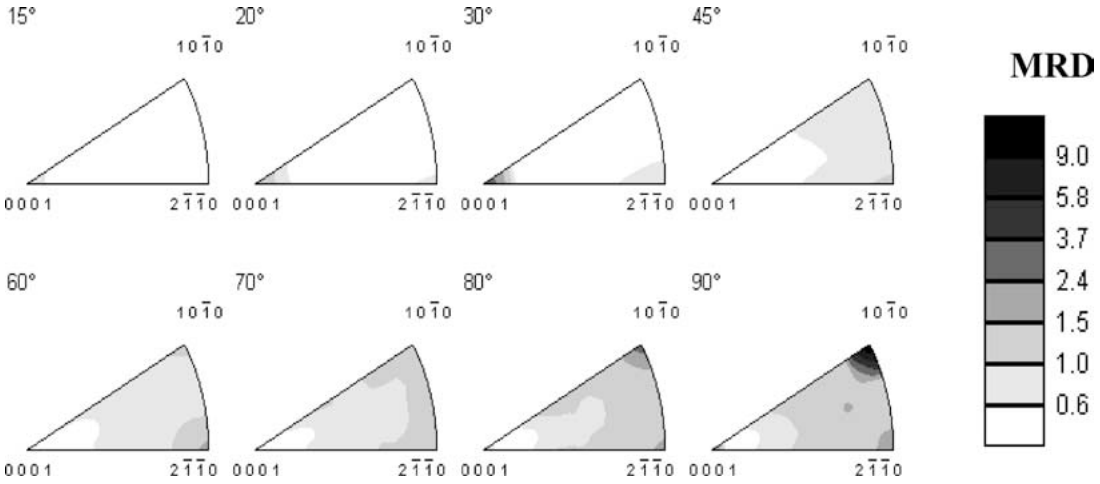

Figure 4. WC-WC grain boundary misorientation distribution in axis angle space. Sections of the fundamental zone are taken perpendicular to the [0001] axis.

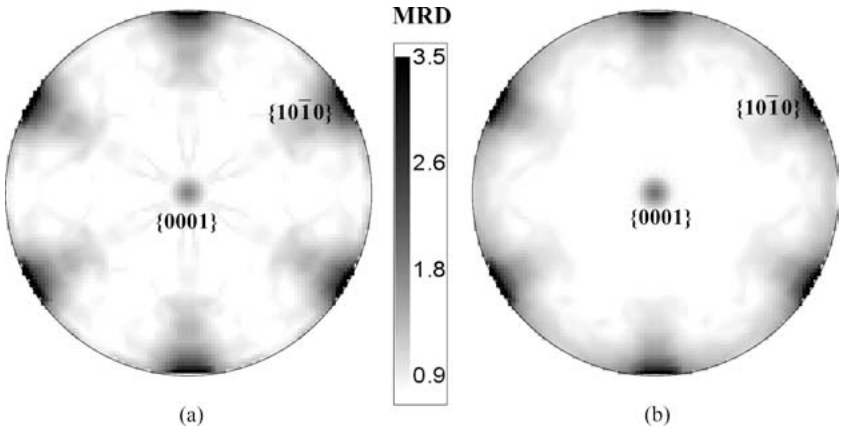

Figure 5. Habit plane probability distribution derived from (a) 50 and (b) 150 crystals. Both are plotted in the [0001] stereographic projection.

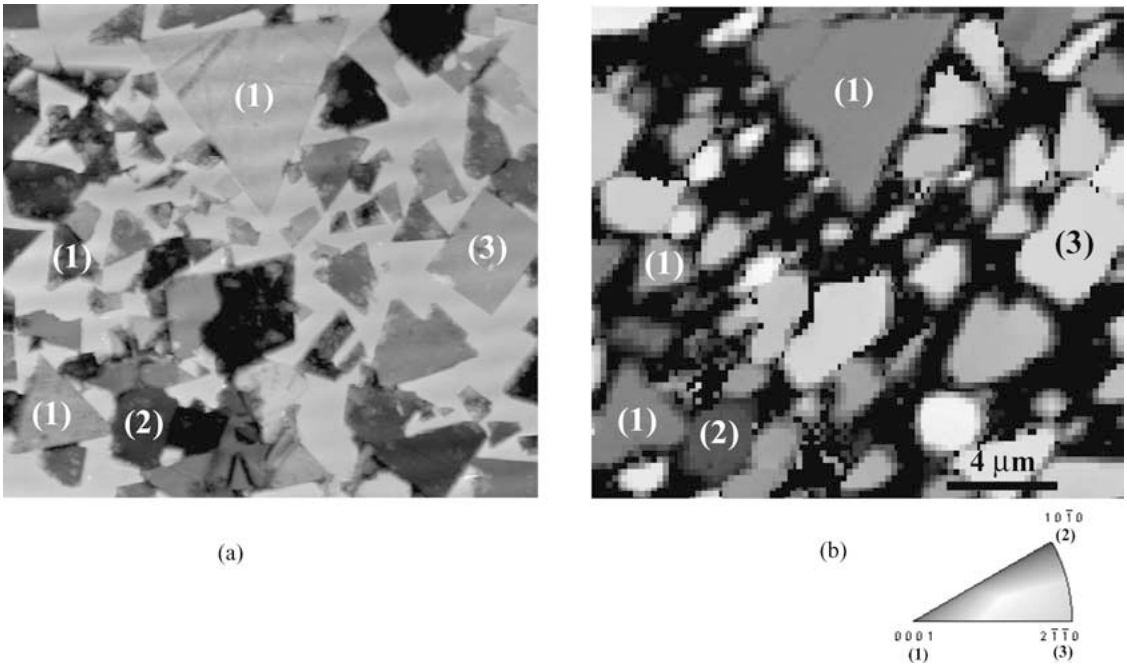

Figure 6. Comparison of WC crystal shape in (a) AFM topography image and (b) OIM inverse pole figure (IPF) map showing the crystal orientation. Both sections are from 20 w/o Co sample. Triangular crystals oriented with [0001] perpendicular to the paper are labeled (1).

symmetry of each crystal. The habit plane distribution for the crystals comprising boundaries with 90° rotations about the [10$\bar{1}$0] axis are depicted in Fig. 8(a). It is clear that the habit of this boundary is on the {10$\bar{1}$0} plane, which is perpendicular to the common rotation axis, [10$\bar{1}$0]. As long as the interface plane is perpendicular to the bicrystal's common rotation axis, then the bounding plane is the same in both crystals and it is a pure twist configuration. If there was a tilt component, the boundary could not be constructed from only {10$\bar{1}$0} planes. The bicrystal formed by a 90° [10$\bar{1}$0] twist is illustrated schematically in Fig. 9(a).

The boundaries with 30° rotations around the [0001] axis, on the other hand, exhibit multiple habit planes, as illustrated in Fig. 8(b). The peak at the basal position confirms the presence of twist boundaries. As mentioned above, as long as the interface plane is perpendicular to the common axis, it is a twist boundary. This

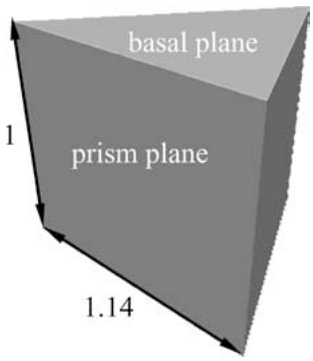

Figure 7. The proposed average shape of a WC crystal in Co.

configuration is illustrated in Fig. 9(b). The remaining habit planes are $\{10\bar{1}0\}$ and $\{11\bar{2}0\}$. The normals to these planes are perpendicular to the [0001] misorientation axis and separated by 30° (the misorientation angle). Therefore, they are complementary planes that comprise the same 30° tilt boundary. In other words, when one crystal is terminated by a $\{10\bar{1}0\}$ plane, the geometrically required complement (parallel plane) in the crystal rotated by 30° around [0001] is $\{11\bar{2}0\}$. Therefore, both of the two habit planes perpendicular to the [0001] axis can be accounted for by the same asymmetric tilt bicrystal, illustrated in Fig. 9(c).

Discussion

The vast majority of the WC-Co boundary traces are consistent with crystal terminations along $\{10\bar{1}0\}$ and $\{0001\}$ planes and from this, we conclude that the average shape of a WC crystal in Co is an approximately equiaxed trigonal prism. Since this conclusion is consistent with earlier observations of deep etched samples [4], the stereological analysis (which had not before been applied to actual experimental observations) is assumed to be reliable [3]. It should be kept in mind that the result from our analysis is merely an average shape; in the composite the WC crystals are always in contact with other crystals and the shape is, therefore, truncated from the idealized form. What we can be certain of from the current results is that approximately two thirds of the WC in contact with Co has a $\{10\bar{1}0\}$ orientation and the remainder has the $\{0001\}$ orientation.

The observed trigonal symmetry of the crystal habit presumably derives from the polarity of the prism faces [5]. If one terminates the WC structure by breaking the fewest number of bonds, then the atoms on the six $\{10\bar{1}0\}$ faces each retain four nearest neighbors (see Fig. 10(a)). However, there are now two distinct sets of prism faces: three terminated by W and three terminated by C; either set of three can form the observed triangular prism. As long as one of the two terminations is more stable than the other in contact with Co, then the observed trigonal shape is expected. Based on the current data, it is not possible to say which of the terminations is observed (see Fig. 10(b) and (c)).

If the trigonal prism is the equilibrium shape, then the Wulff construction can be used to determine the anisotropy of the WC-Co surface energy. However, we have to consider the fact that the WC crystals were coarsening at the processing temperature. In other

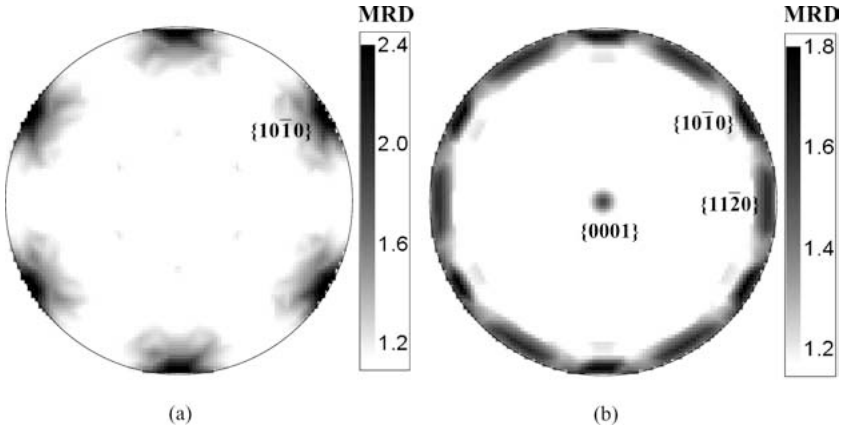

Figure 8. Habit plane probability distribution for (a) 90° $[10\bar{1}0]$ boundaries and (b) 30° [0001] boundaries. Both are plotted in the [0001] stereographic projection.

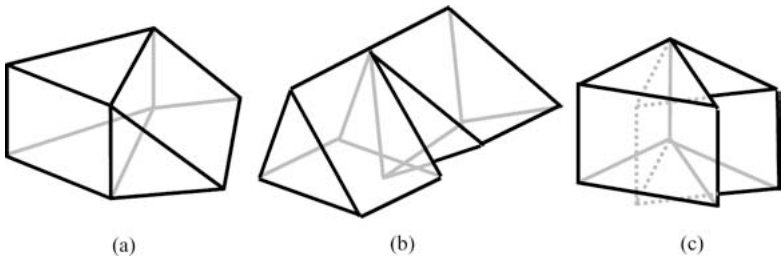

Figure 9. Schematic representations of the three most common types of grain boundaries in the composites. (a) 90° [10$\bar{1}$0] boundary with two {10$\bar{1}$0} planes, (b) 30° [0001] boundary with two {0001} planes and (c) 30° [0001] boundary with {10$\bar{1}$0} and {11$\bar{2}$0} planes. In each case, the complete range of MRD values extends down to 0.6. For clarity, only the upper values are plotted.

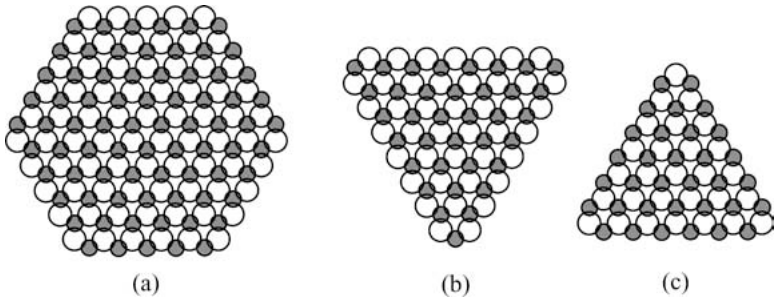

Figure 10. Atomic models for the chemical termination of WC prism planes. The smaller shaded circles represent C and the larger open circles represent W. (a) hexagonal shape with both C and W terminated surface, and (b), (c) two possible trigonal shapes with W and C terminated surfaces, respectively.

words, the smaller crystals were dissolving and the larger crystals were growing. If the rate at which material is redistributed on a given crystal is greater than the rate at which material is transported to or from the crystal, then all of the crystals will have an equilibrium shape determined by the anisotropy of the surface energy. In this case, the shape should not depend on size. On the other hand, if the rates are reversed, then the crystals might adopt shapes characteristic of dissolution and growth. In this case, small dissolving crystals might have different shapes from larger growing crystals. We have found that when we determine the crystal shape from the smallest 20% of the crystals and the largest 20% of crystals, the shapes are indistinguishable from each other and from the shape determined using all of the data. This implies that either the crystals are in an equilibrium shape, or that the growth and dissolution forms are indistinguishable. Assuming that they do adopt their equilibrium shape, then the ratio of the perpendicular distances from the center of the crystal to the faces can be used as a measure of the surface energy anisotropy. In this case, the data indicates that $\gamma_{(0001)}/\gamma_{\{10\bar{1}0\}} = 1.52$.

The analysis presented in the previous section illustrates that three particular grain boundaries occur with a frequency that is much higher than random. These are the 90° [10$\bar{1}$0] twist boundary, the 30° [0001] twist boundary, and the 30° [0001] asymmetric tilt boundary terminated by {10$\bar{1}$0} and {11$\bar{2}$0} planes. Using a tolerance of 3° on the axis and angle parameters and 5° tolerance on the boundary plane parameters, we find that 11% of all the observed boundaries have the 90° [10$\bar{1}$0] twist configuration and 3% have one of the two 30° [0001] configurations. One can imagine several possible mechanisms for the formation of the WC-WC grain boundaries. They might be left over from the starting materials or they might form when two grains impinge as the result of either coarsening or grain growth. Neither process suggests a mechanism for creating higher populations of certain boundary types. A more likely explanation is that a random distribution of boundaries is created by growth related impingement and that the highest energy boundaries are then eliminated from the population by the infiltration of Co. This process, which is consistent with the observed random orientation texture of the samples, would lead to an enhanced

population of boundaries that are resistant to wetting [11]. The boundaries that are preserved in the population have energies that are less than twice the WC-Co interface energy.

Based on the special geometric characteristics of the three boundaries that dominate the population, it seems feasible that they represent relatively low energy configurations and resist wetting. The most populous boundary is the 90° $[10\bar{1}0]$ twist boundary. The WC unit cell has a c/a ratio of 0.976 so that a 90° rotation about $[10\bar{1}0]$ that brings [0001] axis in one crystal parallel to [1000] in the other and the misfit between the two rectangular surface units is less than 3%. The stability of this boundary against wetting has been demonstrated in a TEM study, which showed a direct WC to WC transition at this boundary [7]. The 30° [0001] twist configuration is close to a relatively high coincidence boundary (Σ13, 28° [0001], in which one out of 13 lattice sites are in coincidence). If we assume that the high coincidence also leads to a low energy, then this can potentially explain its stability against wetting. However, the 30° [0001] asymmetric tilt, while it forms the same coincident site lattice, does not have an interface plane of high coincidence.

A second geometric principal that can be used to assess the relative energies of grain boundaries is that interfaces made up of planes with large interplanar spacings generally have lower energies [12]. The basic idea is that planes with large interplanar spacing are also relatively flatter, and two smooth surfaces fit together better than two rough surfaces. The superior fit results in greater attractive forces across the boundary and less repulsion, which means that the boundary has a relatively lower energy. For the case of WC, the $\{10\bar{1}0\}$ and {0001} interface planes have the two greatest interplanar spacings, 2.52 Å and 2.84 Å, respectively. The $\{11\bar{2}0\}$ plane, which is a component of the [0001] asymmetric tilt boundary, has the fourth largest interplanar spacing, 1.45 Å. Therefore, if we assess the energies of the boundaries according to the interplanar spacings of their component planes, we also conclude that three most common boundaries have relatively low energies.

Another potential explanation for the occurrence of a high population of boundaries with $\{10\bar{1}0\}$ and {0001} interface planes is that the crystals are already terminated by these orientations in the liquid Co and, if forced together, would be expected to align with their habit planes parallel. This process would clearly favor the occurrence of $[10\bar{1}0]$ and [0001] twist boundaries. However, since these twist boundaries are observed preferentially at characteristic angles (90° and 30°), the crystals would also have to rotate into these particular configurations. Considering the constraints imposed by the other crystals in the composite, this does not seem very likely. Therefore, an enhanced stability against wetting seems to be a more likely explanation for the high population of these boundaries.

Summary

A stereological analysis has been used to study the types of interfaces that occur in WC-Co composites. As expected, the average WC crystal shape is found to be a roughly equiaxed trigonal prism bound by three $\{10\bar{1}0\}$ prism facets and two {0001} basal facets. Analysis of the misorientation distribution of grain boundaries shows a preference for three particular types of boundaries: 90° $[10\bar{1}0]$ twist boundaries, 30° [0001] twist boundaries and a 30° [0001] asymmetric tilt boundary comprised of complementary $\{10\bar{1}0\}$ and $\{11\bar{2}0\}$ planes. The enhanced population of these grain boundaries probably results from their stability against wetting by Co.

Acknowledgments

This work was supported primarily by Kennametal Incorporated and the Pennsylvania Technology Infrastructure Authority. Partial support by the MRSEC program of the National Science Foundation under Award Number DMR-0079996 is also acknowledged. The authors thank David M. Saylor (NIST) for valuable discussions.

References

1. H.E. Exner, International Metals Reviews (4), 149 (1979).
2. J. Gurland, International Materials Reviews **33**(3), 151 (1988).
3. D.M. Saylor and G.S. Rohrer, J. Amer. Ceram. Soc. **85**, 2799 (2002).
4. J. Wasen and R. Warren, Mater. Sci. and Technol. **5**, 222 (1989).
5. D.N. French, Int. J. Powder Metal. **5**(3), 47 (1969).
6. R. Deshmukh and J. Gurland, Metallography **15**, 383 (1982).
7. S. Hagege, G. Nouet, and P. Delavignette, Phys. Stat. Sol. (a) **61**, 97 (1980).
8. A. Henjered, M. Hellsing, H.-O. Andren, and H. Norden, Mater. Sci. and Technol. **2**, 847 (1986).
9. M.G. Kendall and P.A.P. Moran, *Geometrical Probability* (Hafner Publishing Company, New York, 1963), p. 78.
10. A. Morawiec, J. Appl. Cryst. **28**, 289 (1995).
11. P. Wynblatt and M. Takashima, Interface Science **9**, 265 (2001).
12. D. Wolf, J. Mater. Res. **5**, 1708 (1990).